Available online at www.sciencedirect.com
ScienceDirect
Geochimica et Cosmochimica Acta 74 (2010) 1256–1267
Geochimica et Cosmochimica Acta
www.elsevier.com/locate/gca

The role of background electrolytes on the kinetics and mechanism of calcite dissolution

E. Ruiz-Agudo *, M. Kowacz, C.V. Putnis, A. Putnis

Institut für Mineralogie, University of Münster, Corrensstrasse 24, 48149 Münster, Germany

Received 17 June 2009; accepted in revised form 26 October 2009; available online 10 November 2009

Abstract

The influence of background electrolytes on the mechanism and kinetics of calcite dissolution was investigated using in situ Atomic Force Microscopy (AFM). Experiments were carried out far from equilibrium by passing alkali halide salt (NaCl, NaF, NaI, KCl and LiCl) solutions over calcite cleavage surfaces. This AFM study shows that all the electrolytes tested enhance the calcite dissolution rate. The effect and its magnitude is determined by the nature and concentration of the electrolyte solution. Changes in morphology of dissolution etch pits and dissolution rates are interpreted in terms of modification in water structure dynamics (i.e. in the activation energy barrier of breaking water–water interactions), as well as solute and surface hydration induced by the presence of different ions in solution. At low ionic strength, stabilization of water hydration shells of calcium ions by non-paired electrolytes leads to a reduction in the calcite dissolution rate compared to pure water. At high ionic strength, salts with a common anion yield similar dissolution rates, increasing in the order $Cl^- < I^- < F^-$ for salts with a common cation due to an increasing mobility of water around the calcium ion. Changes in etch pit morphology observed in the presence of F^- and Li^+ are explained by stabilization of etch pit edges bonded by like-charged ions and ion incorporation, respectively. As previously reported and confirmed here for the case of F^-, highly hydrated ions increased the etch pit nucleation density on calcite surfaces compared to pure water. This may be related to a reduction in the energy barrier for etch pit nucleation due to disruption of the surface hydration layer.

1. INTRODUCTION

Weathering of silicates and carbonates plays an important role in controlling the geochemistry of the Earth. The rate of dissolution of these minerals is critical for geochemical cycles, Earth climate feedback and, ultimately, the evolution of the biosphere. This has inspired research on mineral dissolution rates and mechanisms for more than 50 years. Knowledge of mineral dissolution rates under different experimental conditions allows a better description of mineral–water interactions in natural systems. In particular, the dissolution of calcite has spawned a great deal of research due to its importance in a wide variety of processes such as rock and building stone weathering, soil chemistry, and biomineralization. Hence, knowledge of dissolution rates under conditions similar to those occurring in nature is of great interest.

For this reason, research over the last decades has focused on the influence of temperature, CO_2 partial pressure and the presence of foreign substances on calcite dissolution rates. In particular, the influence of both inorganic and organic impurities on calcite dissolution have been frequently addressed in the literature (Barwise et al., 1990; Morse and Arvidson, 2002; Kanellopoulou and Koutsoukos, 2003; Ruiz-Agudo et al., 2009). Commonly, water in contact with rock forming minerals contains significant and variable amounts of ions in solution. The effect of such ions or the so-called *ionic strength* (IS) effect (Buhmann and Dreybrodt, 1987) on mineral dissolution rates has been traditionally ascribed to changes in solubility. The ionic strength (IS) of a salt solution is defined as $IS = \frac{1}{2} \cdot [\sum_i c_i \cdot z_i^2]$, where c_i is the concentration of each ion and z_i is the charge on each ion. The strong long-range electric

* Corresponding author. Tel./fax: +49 0251 83 36107.
E-mail address: eruiz_01@uni-muenster.de (E. Ruiz-Agudo).

0016-7037/$ - see front matter © 2009 Elsevier Ltd. All rights reserved.
doi:10.1016/j.gca.2009.11.004

fields emanating from the ions of the background electrolyte reduce the activity of the mineral constituent ions due to charge screening and therefore, increase the solubility. Thus, considering purely thermodynamic effects, mineral dissolution rates in the presence of electrolytes should increase due to the decrease free energy of the system. However, variations in dissolution rates in the presence of background electrolytes due to changes in the rate at which solute ions leave the crystal are frequently not considered. Experimental studies performed on different mineral have shown that the dependence of growth or dissolution rates on ionic strength is complex. For example, the dissolution rate of quartz increases 100-fold in the presence of cationic solutes such as Na^+ or Ca^{2+}, whereas dissolution rates of other silicate minerals remain mostly unaffected by the introduction of electrolytes (Dove et al., 2005). Relatively few studies have examined the specific effect of ionic strength on calcite dissolution rates, and they offer contradicting reports: Buhmann and Dreybrodt (1987) and Pokrovsky et al. (2005) report no significant effect of IS on calcite dissolution rates (up to 1 M NaCl), whereas Gledhill and Morse (2006) report that an increase in IS of the solution results in decreasing dissolution rates. However, differences among these studies could be related to the use of different experimental conditions, as Gledhill and Morse (2006) used higher pCO_2 and saturation states. NaCl and KCl are the common monovalent salts used to generate IS in mineral dissolution or growth experiments. Ruiz-Agudo et al. (2009) have found significant differences in calcite dissolution rates between solutions of different electrolytes at similar IS. A similar finding was reported for calcium oxalate growth (Weaver et al., 2007), suggesting that the presence of some cations causes higher growth rates than others (at a constant ionic strength and solution saturation), but no clear explanation was provided for this observation. These examples clearly indicate that the effect of ionic strength is not independent of the ionic species generating it. Continuum electrostatics models such as Debye–Hückel (i.e. those considering the ions as point charges) predict the dependence of some parameters (e.g. activity coefficients and solubility) on ionic strength regardless of the surface charge density of the species in solution but, as shown above, there is experimental evidence that ions with high or low surface charge density exert different effects on mineral dissolution and growth which cannot be explained by these models (Collins, 1997).

Recently, Kowacz and Putnis (2008) proposed a model that explains the effect of electrolytes on the kinetics of barite growth and dissolution based on the ability of ions to modify solvent structure dynamics (i.e. the activation energy barrier of breaking water–water interactions) and solute hydration. These authors demonstrated that barite growth and dissolution rates (at constant driving force) are modified in the presence of different background electrolytes, and these variations are related to the hydration characteristics of the different ions. They suggest that changes in the morphology of dissolution features can also be related to changes in the hydration of mineral constituents in the presence of foreign ions in solution, in contrast with the commonly accepted view of specific interactions with active sites on mineral surfaces. In this paper, we address the basic hypothesis that mineral dissolution is governed by complex interactions between solvent structure, surface hydration and ion solvation environment induced by the presence of electrolytes.

To our knowledge, there have been no systematic study aimed at elucidating the mechanisms by which different monovalent ions modify the reactivity of calcite surfaces. As suggested by Teng and Dove (1997) dissolution features may reflect the stabilization of a crystal during mineral growth, with the advantage that dissolution experiments are less difficult and time-consuming than growth studies. To test whether the model proposed by Kowacz and Putnis (2008) for barite applies to the dissolution of calcite, in situ dissolution experiments were conducted using Atomic Force Microscopy (AFM) in the presence of different background electrolytes (NaCl, NaF, NaI, KCl and LiCl) to simultaneously measure dissolution rates and observe the surface topography. Changes in etch pit nucleation density induced by the presence of electrolytes, frequently not reported in mineral dissolution studies, are also discussed.

2. METHODOLOGY

Freshly cleaved calcite $\{1\,0\,\bar{1}\,4\}$ surfaces (Iceland spar, Chihuahua, Mexico), ca. $3 \times 3 \times 1$ mm in size, were used as substrates for AFM dissolution experiments. Before each dissolution experiment, deionized water was passed over the crystal to clean the cleaved surface, as well as to adjust the AFM operating parameters as in Arvidson et al. (2006). Five saline systems were used in the in situ AFM dissolution experiments: NaF, NaCl, NaI, LiCl and KCl. Solutions were prepared from high-purity anhydrous solids (Panreac, reagent grade) dissolved in deionized water (resistivity $> 18\ m\Omega\ cm^{-1}$). Table 1 shows experimental conditions for each saline solution. The absence of calcium in the input saline solutions ensured constant far-from-equilibrium conditions with respect to calcite during the experiments. Solutions were prepared immediately before the experiments, with no time to equilibrate with the ambient atmosphere and thus the amount of carbonate and bicarbonate ions in solutions is considered to be negligible. Calcium-free saline solutions in concentrations ranging from 1 mM to 100 mM flowed continuously for 30 min at $50\ mL\ h^{-1}$ from a syringe coupled to an O-ring-sealed fluid cell containing the sample crystal. Shiraki et al. (2000) have shown that for $pH > 5.3$ the velocity of step retreat is independent of flow rate for values higher than $29\ mL\ h^{-1}$ (at room T and $pCO_2 \approx 10^{-3.5}$ atm). Furthermore, Arvidson et al. (2003) demonstrated that surface reaction kinetics control calcite dissolution far-from-equilibrium conditions at circum-neutral pH, similar to the conditions of our experiments). Therefore, the flow rate used guarantees that dissolution rates measured are surface controlled.

In situ observations and measurements of the $\{1\,0\,\bar{1}\,4\}$ calcite surfaces during dissolution were performed using a closed fluid cell of a Digital Instruments Nanoscope III Multimode AFM working in contact mode under ambient conditions ($t = 20$ °C). The scanning frequency was 4 Hz, giving an average of 1.5 scans per min over 25 (5×5) and 100 (10×10) μm^2. AFM images were collected using

Table 1
Etch pit spreading rates of calcite (nm s^{-1}) as a function of ionic strength (IS, mM) for different background electrolytes.

LiCl				NaF				NaI			
IS	pH	Rate	Std	IS	pH	Rate	Std	IS	pH	Rate	Std
0						1.99	0.14				
1	6.63	1.73	0.10	1	6.02	4.23	0.15	1	6.12	2.35	0.17
5	6.58	2.10	0.41	5	6.18	4.30	0.63	5	6.18	2.14	0.05
10	6.57	2.68	0.16	10	6.28	6.12	0.09	10	6.25	3.16	0.16
50	6.63	2.68	0.12	50				50	6.23	3.62	0.28
100	6.70	3.04	0.08	100				100	6.45	4.19	0.09

KCl				NaCl			
IS	pH	Rate	Std	IS	pH	Rate	Std
0						1.99	0.14
1	5.69	2.82	0.08	1	6.80	1.96	0.17
10	5.52	2.12	0.05	5	7.00	1.62	0.24
100	5.54	3.23	0.14	20	6.90	2.88	0.46
				100	7.00	3.17	0.16

Si_3N_4 tips (Veeco Instruments, tip model NP-S20) with spring constants of 0.12 N m^{-1} or 0.58 N m^{-1}. Images were analyzed using the NanoScope software (Version 5.31r1). Measurements of step retreat velocity (or etch pit spreading rate) were made from sequential images scanned in the same direction. The retreat velocity given by v_{sum} (nm s^{-1}) $= (v_+ + v_-)$ (where v_+ and v_- are the retreat velocities of + and − steps, respectively) was calculated by measuring the length increase per unit time between opposite parallel steps in sequential images.

In flow through experiments performed in AFM, variations and uncertainties related to the reacting surface area contribute to significant error in macroscopic rate determinations (De Giudici, 2002), typically leading to an overestimation of macroscopic dissolution rates (Duckworth and Martin, 2004). Unfortunately, the very low amount of calcium in the outlet solution (a few mmol L^{-1}) (Arvidson et al., 2006) precludes obtaining reliable concentration values and, thus, dissolution rates, R_{AFM} (mol cm^{-2} s^{-1}), were calculated as in Ruiz-Agudo et al. (2009), using the equation:

$$R_{AFM} = x_A \frac{\Delta V}{A V_m t} \quad (1)$$

where ΔV (cm^3) is the volume increase of a given etch pit in time-sequence AFM images over a given area of calcite (molar volume of calcite, $V_m = 36.93$ cm^3 mol^{-1}), A (cm^2) is the surface area of the etch pit, x_A is the fractional area occupied by all etch pits in a given image, t (s) is the time interval between sequential images. ΔV was determined by measuring depth and area increments of individual etch pits on a given pair of sequential AFM images.

3. RESULTS

3.1. Dissolution features on (10 $\bar{1}$ 4) calcite surfaces

Calcite dissolution occurs via etch pit formation on (1 0 $\bar{1}$ 4) surfaces after the injection of deionized water into the fluid cell. Dissolution pits (etch pit density $\sim 1.2 \times 10^8$ cm^{-2}) were shallow and displayed the typical rhombohedral shape that has been thoroughly described (Arvidson et al., 2006 and refs. therein) (Fig. 1a). In the presence of NaF, etch pits lost their characteristic rhombohedral shape, and became elongated, acquiring a more or less elliptical or pseudohexagonal appearance (Fig. 1b–f). The etch pits developed new straight edges parallel to [2 $\bar{2}$ 1], i.e. to the elongation direction (Fig. 2). Additionally, we observed a general increase in etch pit density with increasing NaF concentration (Fig. 1b–f). Calcite dissolution in NaF 0.05 M solutions resulted in a ~20-fold increase in the observed etch pit density ($\sim 2.5 \times 10^9$ cm^{-2}) compared with water. A slight increase in etch pit density was also observed in the presence of Li^+ with increasing ionic strength ($\sim 2.2 \times 10^8$ cm^{-2}). In the presence of LiCl, a new step edge developed parallel to [0 1 0] intersecting [$\bar{4}$ 4 1]_ and [4 8 $\bar{1}$]_ steps (Fig. 3). This effect is ascribed to the presence of Li^+, as it was not observed in other Cl-bearing solutions. A similar change in etch pit morphology was also detected, although to a lesser extent, in NaI solutions. Increasing the NaCl or KCl concentration did not result in a substantial difference in etch pit density relative to deionized water, and the dissolution took place mainly as a layer-by-layer process, with pits nucleating and spreading on calcite (1 0 $\bar{1}$ 4) planes. The morphology of etch pits developed in the presence of both salts was very similar to those that developed in pure water.

In pure water, the length ratio of the rhombus diagonals [0 1 0] and [2 $\bar{2}$ 1] is 0.80 ± 0.06. This parameter is a useful indicator of the impact of increasing ionic strength on etch pit morphology. Fig. 4 shows a plot of the length ratio as a function of the ionic strength for the different salts tested. NaCl and KCl did not induce significant changes in this parameter in the range of ionic strength tested. In contrast, NaF considerably reduced the [0 1 0]/[2 $\bar{2}$ 1] values with increasing IS (from 0.80 ± 0.06 to 0.26 ± 0.03 at IS = 10 mM). LiCl and NaI had a similar effect, although in both cases the reduction was less pronounced (0.50 ± 0.06 and 0.62 ± 0.04 nm/s, respectively). These results are consistent with observed changes in etch pit morphology induced by NaF, LiCl, and NaI.

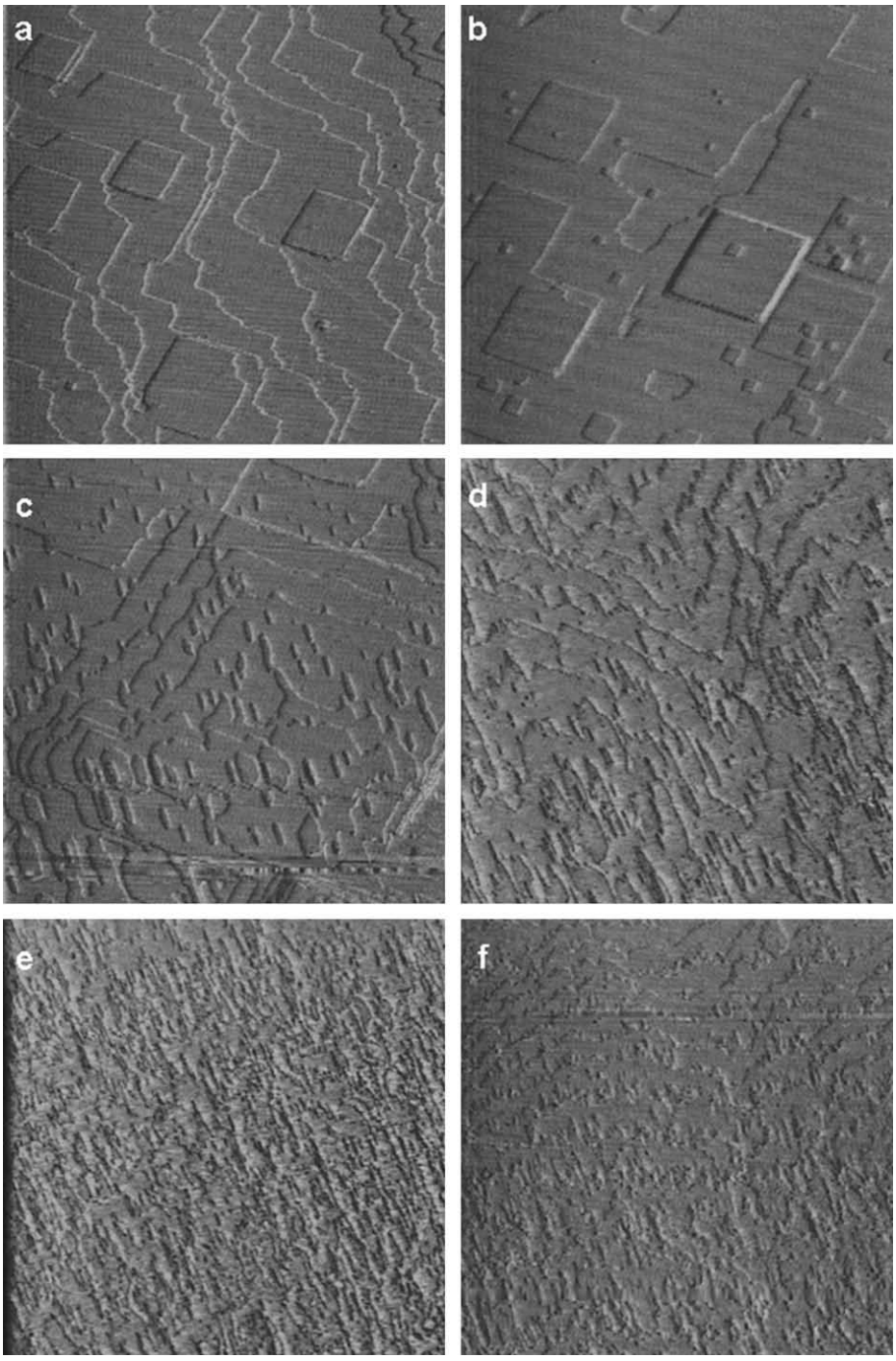

Fig. 1. AFM height images of calcite cleavage surfaces 2 min after injection and flow of (a) deionized water and NaF at concentrations of (b) 1 mM, (c) 10 mM, (d) 20 mM, (e) 50 mM and (f) 500 mM. Note the high etch pit nucleation density achieved at concentrations >20 mM NaF. Image size: 5 × 5 μm.

3.2. Etch pit spreading rates

The average etch pit spreading velocity, v_{sum} (i.e. the rate of change in etch pit length along $[\overline{4}\,4\,1]$ or $[4\,8\,\overline{1}]$, sum of the retreat velocity of opposite + and − steps, $v_+ + v_-$) in deionized water was 1.99 ± 0.14 nm s^{-1}. Table 1 and Fig. 5 show v_{sum} as a function of IS for the electrolytes tested. The step retreat rate generally increased with increasing IS for all the salts tested after going through a minimum at relatively low IS. The average etch pit spreading velocity on the calcite cleavage surface varied according to the nature of the background electrolyte at a low and constant ionic strength (0.001 M), increasing in the order LiCl < NaCl < NaI < KCl < NaF. Note that the spreading rate in 1 mM LiCl and 5 mM NaCl solutions reached slightly lower values than that observed in pure water. This

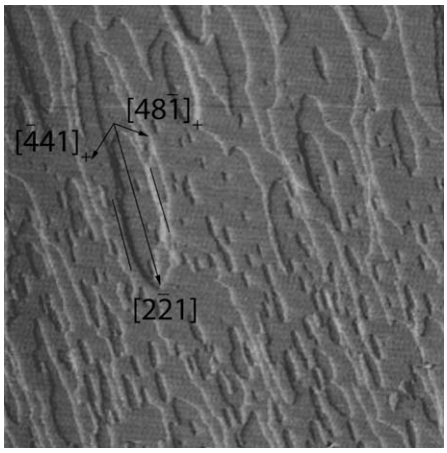

Fig. 2. AFM deflection image of etch pits formed in the presence of 10 mM NaF. New edges parallel to [2 $\bar{2}$ 1], absent in pure water, are observed, change the etch pit morphology from rhombohedral to pseudohexagonal or elliptical. Image size: 5 × 5 μm.

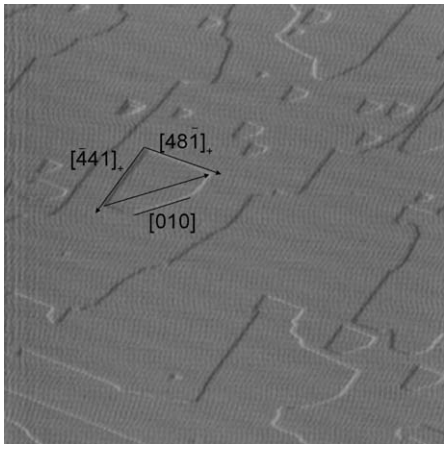

Fig. 3. AFM deflection image of etch pits formed in the presence of 100 mM LiCl. A new edge parallel to [0 1 0], absent in pure water, is observed. Image size: 5 × 5 μm.

indicates some degree of inhibition of calcite dissolution at low ionic strength in the presence of these salts which will be discussed in detail in Section 4. In general, the dissolution rate increased with ionic strength for all salts tested. It is interesting to note that the smallest increase in the dissolution rate was found for KCl (from 2.82 to 3.23 nm/s at IS = 0.001 and 0.100 M, respectively). In concentrated saline solutions (IS = 0.100 M), the etch pit spreading rate v_{sum} increased in the order LiCl ≈ NaCl ≈ KCl < NaI(<NaF). It is important to note that at NaF concentrations above 10 mM, it was not possible to quantify the etch pit spreading rate as they coalesced faster than the scanning rate, due to the high etch pit density and their fast propagation rate.

$v_{2\bar{2}1}$ (i.e. etch pit spreading rate along the [2 $\bar{2}$ 1] diagonal) and v_{010} (i.e. etch pit spreading rate along the [0 1 0] diagonal) behave similarly to v_{sum}. After going through a minimum, they increased with IS in NaCl and KCl. In contrast, NaF markedly reduced v_{010} (from 3.10 ± 0.24 – in pure water – to 1.66 ± 0.26 nm/s – in 10 mM NaF-), indicating an elongation of the etch pits along the [2 $\bar{2}$ 1] diagonal. It was also observed that in the presence of NaI and LiCl the spreading rate along the [0 1 0] diagonal remained unchanged upon increasing the IS of the solution.

3.3. Dissolution rates

Table 2 shows calcite dissolution rates calculated from AFM measurements according to Eq. (1). Dissolution rates at both high and low ionic strength follow the same trends observed for etch pit spreading rates (within the experimental error, see Fig. 6). The log of calcite dissolution rate in deionized water was found to be −11.75 (±0.18) mol cm^{-2} s^{-1}, in good agreement with values reported by Arvidson et al. (2003) (−11.68 mol cm^{-2} s^{-1}) and Vinson and Luttge (2005) (−11.10 mol cm^{-2} s^{-1}), as determined using VSI (vertical scanning interferometry). At low IS, the electrolytes tested increased R_{AFM} in the order NaCl ≈ LiCl < NaI < KCl < NaF. Dissolution rates in NaCl and LiCl were similar to those measured in the presence of deionized water. In concentrated saline solutions (IS = 0.100 M), the dissolution rate increased in the order LiCl ≈ NaCl ≈ KCl < NaI(<NaF). Again, calculation of the dissolution rates was not possible for NaF due to the extremely fast coalescence of etch pits. At this ionic strength, the calcite dissolution rate in the presence of KCl was one order of magnitude faster (log R_{AFM} = −10.78 (±0.01) mol cm^{-2} s^{-1}) than in deionized water, but slightly lower than at the lower KCl concentration (−10.62 (±0.00) mol cm^{-2} s^{-1} at IS = 0.001 M).

4. DISCUSSION

4.1. Morphology of dissolution features

The calcite (1 0 $\bar{1}$ 4) surface has three periodic bond chains (PBCs) running along [$\bar{4}$ 4 1], [2 $\bar{2}$ 1], and [0 1 0]. The PBCs along [2 $\bar{2}$ 1] and [0 1 0] are less stable than the PBC along [$\bar{4}$ 4 1]. The four step edges of the etch pits formed on {1 0 $\bar{1}$ 4} faces during dissolution in pure water are parallel to [$\bar{4}$ 4 1]: i.e. they are parallel to [$\bar{4}$ 4 1]$_+$, [4 8 $\bar{1}$]$_+$, [$\bar{4}$ 4 1]$_-$ and [4 8 $\bar{1}$]$_-$ directions. The subscripts (+ or −) follow the convention used by Paquette and Reeder (1995). The etch pits show no edges parallel to [2 $\bar{2}$ 1] and [0 1 0]. Steps parallel to [$\bar{4}$ 4 1] are bonded by alternating Ca^{2+} and CO_3^{2-} ions, while [2 $\bar{2}$ 1] and [0 1 0] steps are bonded by either Ca^{2+} or CO_3^{2-}. The structurally equivalent [$\bar{4}$ 4 1]$_-$ and [4 8 $\bar{1}$]$_-$ steps are acute and intersect the bottom of the etch pit at an angle of 78°, while [$\bar{4}$ 4 1]$_+$ and [4 8 $\bar{1}$]$_+$ steps are obtuse and intersect the bottom of the etch pit at an angle of 102° (Hay et al., 2003). The intersection of etch pit edges results in the formation of three kinds of corners: one acute/acute (−/−), one obtuse/obtuse (+/+) and two mixed corners (−/+).

Changes in morphology of etch pits on calcite cleavage surfaces in the presence of NaF were previously reported by Vavouraki et al. (2009). They concluded that F^- adsorption on calcite steps may be responsible for the change in pit morphology. A similar effect of Cd^{2+} on calcite etch pit

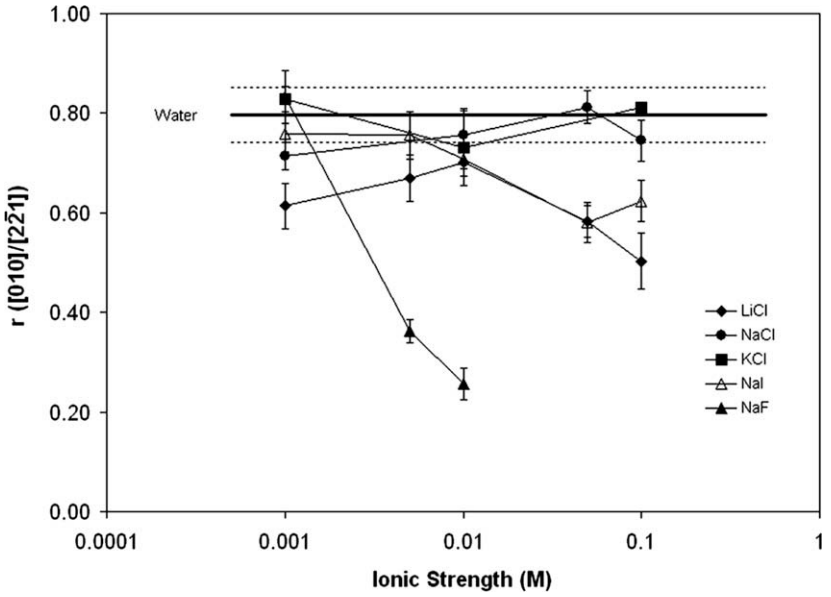

Fig. 4. [0 1 0]/[2 $\bar{2}$ 1] length ratio of etch pits nucleated on calcite {1 0 $\bar{1}$ 4} terraces vs. IS for different background electrolytes: (▲) NaF, (■) KCl, (●) NaCl, (△) NaI, and (♦) LiCl solutions. The straight line represents the value of [0 1 0]/[2 $\bar{2}$ 1] length ratio in pure water and the dashed lines show the error of this measurement.

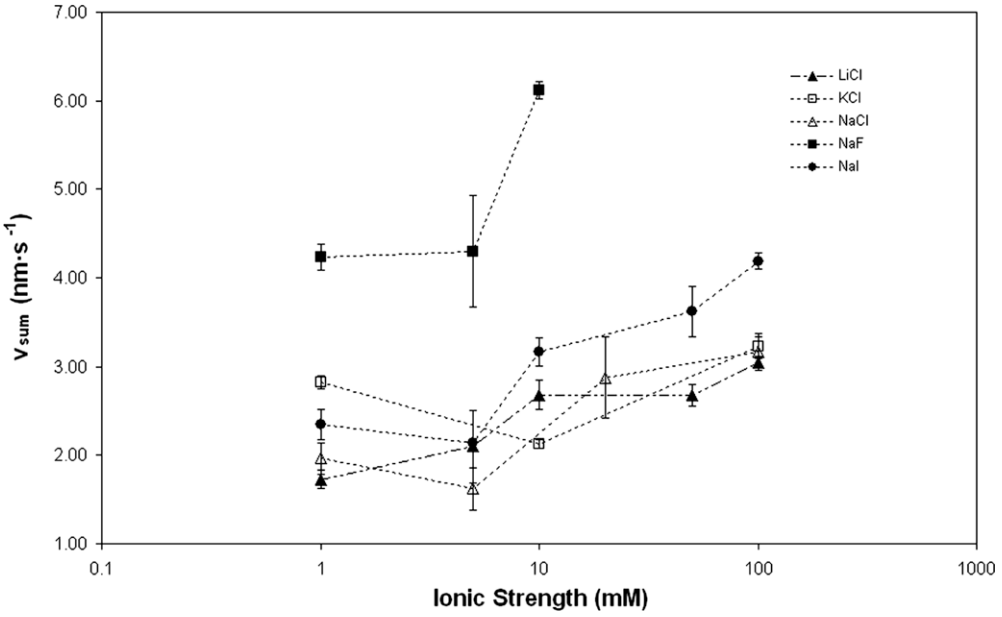

Fig. 5. Average spreading rate of etch pits nucleated on calcite {1 0 $\bar{1}$ 4} terraces vs. IS of (■) NaF, (●) NaI, (□) KCl, (△) NaCl, and (▲) LiCl solutions.

morphology during dissolution was shown by Perez-Garrido et al. (2007). In this case, the effect was attributed to preferential adsorption of the cation on [$\bar{4}$ 4 1]_ and [4 8 $\bar{1}$]_ steps. However, as suggested by Kowacz and Putnis (2008), changes in etch pit morphology may not be solely a consequence of specific interactions between ions and mineral surfaces. Increasing ion hydration by the addition of electrolytes to a solution reduces both repulsive interactions between ions of the same charge and attractive interactions between ions of opposite charges. Hence, the presence of electrolytes will stabilize steps bonded by either CO_3^{2-} or Ca^{2+} (i.e. [2 $\bar{2}$ 1] and [0 1 0] steps) whereas steps bonded by alternating CO_3^{2-} or Ca^{2+} (i.e. those parallel to [$\bar{4}$ 4 1] and the structurally equivalent [4 8 $\bar{1}$]) will be less stable in salt solutions. In this case, variations in etch pit morphology can be explained without considering specific interactions between impurities in solution and the calcite surfaces.

Calcite dissolution in the presence of Li^+ resulted in the development of etch pits with a new step edge parallel to [0 1 0]. The influence of lithium on calcite growth morphol-

Table 2
AFM derived calcite dissolution rates (R_{AFM}, mol cm^{-2} s^{-1}) for the different salts tested at low and high ionic strength (IS, mM).

NaCl			NaF			NaI		
IS	Log rate	Std	IS	Log rate	Std	IS	Log rate	Std
0				−11.75	0.18			
1	−11.74	0.12	1	−10.44	0.02	1	−11.10	0.09
100	−11.06	0.11	100			100	−10.91	0.03

KCl			LiCl		
IS	Log rate	Std	IS	Log rate	Std
0				−11.75	0.18
1	−10.62	0.00	1	−11.16	0.10
100	−10.78	0.01	100	−10.97	0.03

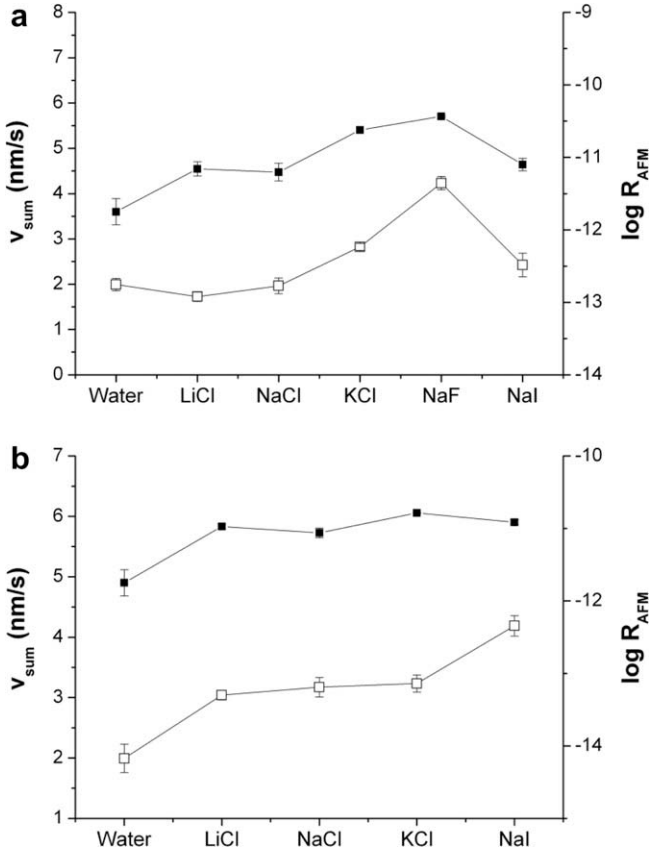

Fig. 6. Etch pit spreading rates (open symbols) vs. dissolution rates (filled symbols) at IS = 0.001 M (a) and IS = 0.1 M (b) for the different electrolytes tested.

ogy was previously described and discussed (Rajam and Mann, 1990) but, to our knowledge, there are no reports on the effect of lithium on calcite dissolution. Rajam and Mann (1990) found that the pinacoid {0 0 0 1} form appears together with the typical {1 0 $\bar{1}$ 4} rhombohedron in calcite crystals growing from Li-bearing solutions. Stabilization of (0 0 0 1) faces is consistent with the development of a new edge parallel to [0 1 0] on calcite etch pits during dissolution since the direction of the new edge corresponds to the intersection of the {0 0 0 1} form with the cleavage rhombohedron {1 0 $\bar{1}$ 4} (Fig. 7). Atomistic simulations of the effects of ions on calcite surfaces revealed that the basal (0 0 0 1) face, unstable under normal (i.e. no impurities or additives) growth conditions, becomes stable in the presence of Li^+ (Titiloye et al., 1993). The negative segregation energy (i.e. the difference in standard chemical potentials of an element between the surface layer and the bulk) of Li^+ ions on the calcite {0 0 0 1} surface from the bulk crystal lattice suggests that during growth lithium ions prefer to remain at surface sites (Titiloye et al., 1993). This is in agree-

ment with results of Rajam and Mann (1990) who, based on X-ray and infrared spectroscopy analyses, reported no significant disruption of the host lattice by Li^+.

The dipolar (0 0 0 1) face consists of alternate layers of Ca^{2+} and CO_3^{2-} ions in successive planes. Carbonate ions are in a non-close packed arrangement and leave interstices of 0.60 Å within planes in which Li^+ may be accommodated (Li^+ ionic radius = 0.59 Å), partially neutralizing the surface dipole of the basal faces and stabilizing them (Rajam and Mann, 1990). The ionic radius of Na^+ (0.99 Å) or K^+ (1.52 Å) is too large for these ions to be accommodated in (0 0 0 1) interstices, in agreement with the absence of significant changes in etch pit morphology in experiments where NaCl or KCl were used as background electrolytes. Pastero et al. (2004, 2005, 2007) interpreted the observed morphological change in terms of adsorption of 2D epitaxial layers of the monoclinic Li_2CO_3 on the {0 0 0 1} form of calcite. However, given its extremely high solubility, the formation of Li_2CO_3 is very unlikely. That stabilization of {0 0 0 1} forms is observed during dissolution experiments suggests that incorporation of Li^+ in the surface layer is a more feasible explanation for the changes in calcite etch pit and growth morphology induced by lithium.

4.2. Etch pit nucleation: role of kosmotrope ions

Ruiz-Agudo et al. (2009) showed that an increase in the rates of calcite dissolution is not always accompanied by an increase in the etch pit spreading rates. As they observed for calcite dissolution in Mg-bearing solutions, increasing the electrolyte concentration results in a net increase in the overall dissolution rate, despite the observed decrease in the propagation rate of the etch pits. Other factors such as etch pit nucleation density or deepening rates also influence overall dissolution rates and must be considered in a systematic study of mineral dissolution. In our case, etch pits were shallow with a depth of one unit cell in the presence of all the salts tested. Dissolution occurred as a layer-by-layer process, and the removal of a surface layer (~3 Å high) was faster than nucleation of new etch pits within pre-existing ones. No significant deepening of the calcite surface exposed to the solution was observed. Therefore, differences result from changes in etch pit nucleation density and/or spreading rate.

Nucleation of etch pits provides a source of kinks and step edges from which the detachment of ions is energetically more favorable compared with detachment from atomically flat surfaces (Liang et al., 1996). Etch pit nucleation on {1 0 $\bar{1}$ 4} calcite surfaces occurs at defects (MacInnis and Brantley, 1992), although at high undersaturation the reduction in the energy barrier for unassisted pit nucleation is sufficient to enable 2D nucleation on defect-free surfaces (Teng, 2004). Therefore, similar etch pit densities should be observed in our experiments as the saturation state was extremely low in all cases. This does not explain why, in the presence of high F^- concentrations, we observed etch pit densities of up to $\sim 2.5 \times 10^9$ cm^{-2} (one order of magnitude higher than in deionized water -1.0×10^8 cm^{-2}). These differences may be explained by the hydration characteristics of the background ions. For a recent review of the effect of background electrolytes on the structure of water see Marcus (2009). Ions with low charge density (*chaotropes* or structure-breakers) seem to have little effect on etch pit density, whereas ions with high charge density (*kosmotropes* or structure-makers) systematically increase the etch pit nucleation density. This effect was observed in the presence of F^- in our experiments, and previously reported for Mg^{2+} (Ruiz-Agudo et al., 2009) and Mn^{2+} (Vinson et al., 2007) as well as for Ca^{2+} in the case of quartz dissolution (Dove et al., 2005). Both Ca^{2+} solvation and hydration of the calcite surface determine the rate of the detachment of building units from the crystal (Stack, 2009). Kosmotrope ions in solution bind the water tightly and cause strong electrostatic ordering of water molecules in their first solvation shell. These ions strongly interact with exposed surfaces, competing for surface water and disrupting the surface hydration layer. This leads to destabilization of calcite surfaces, favoring 2D nucleation of etch pits, and a net increase in the dissolution rate (Arvidson et al., 2006; Vinson et al., 2007; Ruiz-Agudo et al., 2009). Although we would expect a similar behavior in the case of lithium due to its kosmotrope character, it has a weak effect on etch pit nucleation (etch pit density ~ 2.2×10^8 cm^{-2}) because its ability to modify the water structure is small (see Fig. 8).

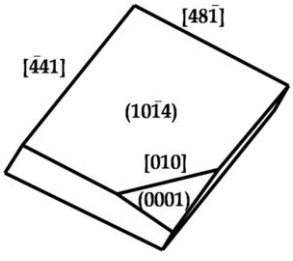

Fig. 7. Simulation of calcite morphology with overdevelopment of the (0 0 0 1) face. The direction [0 1 0] is the intersection between (1 0 $\bar{1}$ 4) and (0 0 0 1) faces.

4.3. Effect of electrolytes on dissolution kinetics

As stated earlier, all the salts tested generated similar dissolution patterns, with no changes in etch pit deepening rates and, with the exception of NaF and LiCl, no significant differences in etch pit density compared to pure water. Hence, variation in dissolution rates resulted from changes in etch pit spreading rates, augmented in the case of LiCl and NaF by the higher etch pit density. As shown in Fig. 6, within experimental uncertainties, dissolution rates calculated from AFM measurements followed similar trends to etch pit spreading rates at both low and high ionic strength. Therefore, the effect of the electrolytes tested on calcite dissolution kinetics can be studied using either of these parameters.

In dilute solutions (low ionic strength), water molecules in the hydration shell of a calcium ion are electrostatically stabilized by the addition of electrolytes. The stabilization results from the electrostatic attraction between water dipoles aligned in the Ca solvation shell and counter ions

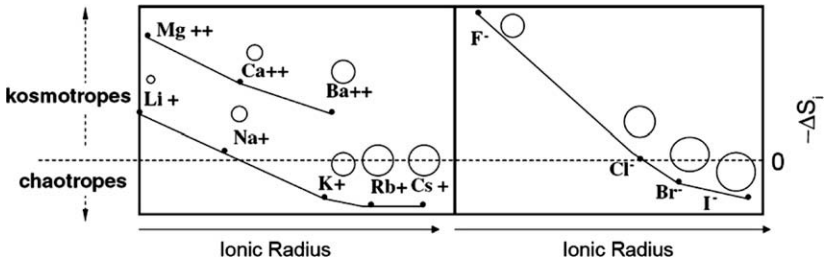

Fig. 8. Hydration characteristics of selected ions (modified from Kowacz et al., 2007). ΔS_i is the difference between the entropy of water near an ion and the entropy of pure water. Positive values of $-\Delta S_i$ indicate that water is less mobile than bulk water, whereas negative values indicate that water is more mobile than bulk water. The dotted line indicates the transition between kosmotropes ($-\Delta S_i$ greater than zero) and chaotropes ($-\Delta S_i$ lower than zero). Circles indicate relative ion radii.

present in solution, lowering the potential energy of the water molecules in their respective hydration shells (Samoilov, 1967, 1971). However, the formation of ion-pairs in solution will reduce the ability of salts to stabilize ion solvation shells. The closer the ions, the more screened are their electric fields and consequently the electrostatic influence on solvation water diminishes. In Fig. 9, etch pit spreading rates were plotted against the difference in the diffusion coefficients of the ionic salt constituents (ΔD). This parameter is a measure of ion separation in solution. The tendency of ions to associate or stay apart in solution depends on their hydration characteristics (Hawlicka and Swiatla-Wojcik, 2003; Collins et al., 2007) and ion hydration, according to kinetic theory, can be described by the activation energy of exchange of water molecules in the environment of the ion (Samoilov, 1965), the quantity that determines ionic diffusion (Lee and Rasaiah, 1996). The dependence of etch pit spreading rates on ΔD follows different trend lines for salts composed of like-hydrated (more associated) and oppositely-hydrated ions (salts composed of kosmotrope–kosmostrope or chaotrope–chaotrope pairs are like-hydrated). Calcite dissolution rates at low IS (0.001 M) decrease with increasing ion separation in solution (decreasing ion-pairing) and thus, with increasing stabilization of water in the cation hydration shell. The lower dissolution rates are therefore expected for the less ion-paired electrolytes (LiCl and NaCl). This contrasts with what was observed during barite dissolution (Kowacz and Putnis, 2008) but may be understood by considering relative differences in entropy (ΔS) during calcite and barite dissolution.

The decrease in the Gibbs free energy on dissolution involves both the enthalpy and entropy changes in the process of breaking the bonds in the crystal structure and subsequent hydration of the constituent ions by water molecules. Stabilization of water molecules on calcium hydration shells by the presence of electrolytes makes the process more exothermic ($\Delta H < 0$) but two entropic effects must

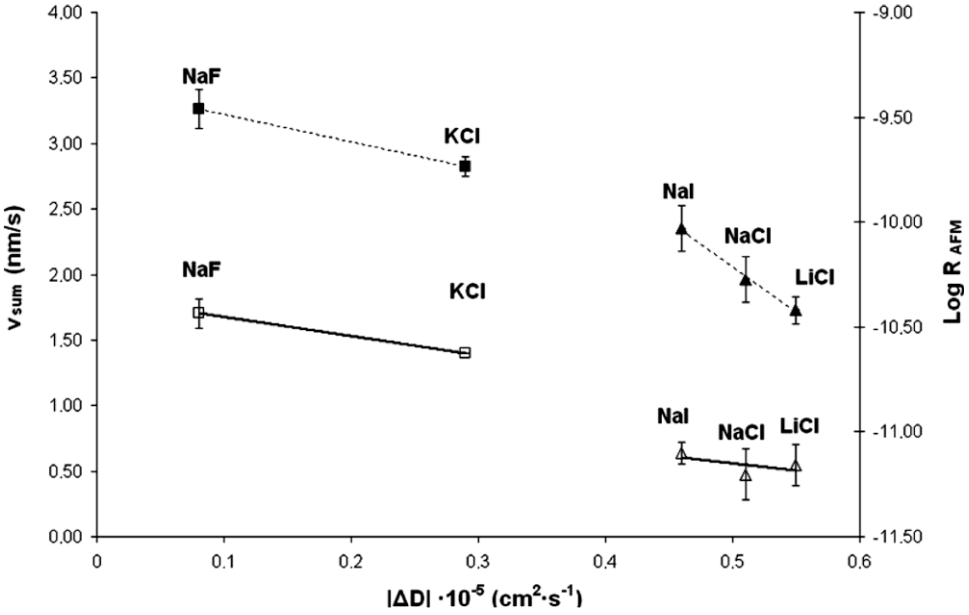

Fig. 9. Etch pit spreading rates (filled symbols) and dissolution rates (empty symbols) at IS = 0.001 M in different background salts as a function of difference in the diffusion coefficients of ionic salt constituents (ΔD). Note that relationships between dissolution rates and ΔD follow different trend lines for salts composed of like-hydrated (i.e. more associated) (squares) and oppositely-hydrated ions (triangles). Diffusion coefficients are taken from Lee and Rasaiah (1996).

also be taken into account. On one hand, there is more disorder as the crystal structure breaks ($\Delta S > 0$) and, on the other hand, there is increased ordering in the water molecules ($\Delta S < 0$), as they arrange around ions in solution. This latter effect is particularly important if the ions are small and highly charged. Hence, Ca^{2+} is much more strongly hydrated than Ba^{2+} and its hydration causes significant order of the solvent molecules attracted by the ion, as inferred by the entropies of solvation of calcium and barium ($\Delta S_{str} = -40$ J mol^{-1} K^{-1} and -10 J mol^{-1} K^{-1}, respectively) that result solely from the interaction of an ion with the water in its environment (Marcus, 1987). This parameter reflects the contribution of water-structuring to the standard molar entropy of the ions, and is calculated at infinite dilution of the solute in the solvent, where solute-solute interactions are absent (Marcus, 1987). The presence of carbonate instead of sulfate ions further augments the calcium water-structuring effect ($\Delta S_{str} = -40$ J mol^{-1} K^{-1} and 20 J mol^{-1} K^{-1} for CO_3^{2-} and SO_4^{2-}, respectively). Thus, the overall change in entropy upon dissolution is smaller for calcite than barite. The stabilization of the hydration waters by the presence of background salts augments the unfavorable entropic effect upon calcite dissolution relative to barite, thus decreasing the overall change in entropy of dissolution.

At higher ionic strengths (100 mM), stabilization by counter ions of hydration water surrounding building units will be counteracted by the presence of like-charges that destabilize the hydration shell by increasing the potential energy of water molecules due to repulsive electrostatic forces between the like-charge ions and water dipoles. Hence, the effect of background ions on water structure dynamics will determine the salt-specific effects on calcite dissolution rates. The observed minimum in the plots of calcite dissolution rates vs. IS (Fig. 5) supports the hypothesis of a competition between electrostatic and hydration forces in the control of dissolution rates in electrolyte solutions. Kowacz and Putnis (2008) demonstrated that, at high ionic strength, dissolution rates of barium sulfate decrease in response to the increased structuring effect of background ions on the aqueous solvent, as more energy is required to break water bonds to hydrate the ions. It also has to be considered that the more structured the solvent the higher the competition for water of hydration between the H-bonded network of water and the solute ions, resulting in an increase in the frequency of water exchange around the latter. This means more positive entropy upon ion hydration and, therefore, a more favorable process. As stated, entropic effects upon calcite dissolution predominate over enthalpic effects due to the high surface charge density of Ca^{2+} sites and the structuring of water molecules around Ca^{2+} in solution. The most significant differences in the dissolution kinetics of calcite are observed in the presence of different background anions. Considering that they will determine solvent structure around Ca^{2+} cations, solvation of the cation is believed to be the rate limiting step in the dissolution of calcite, as suggested by Pokrovsky and Schott (2002) for divalent carbonates and by Dove and Czank (1995) for divalent sulfates. Therefore, salts with a common anion (LiCl, NaCl and KCl) have similar effects on the calcite dissolution rate at high ionic strengths ($v_{sum} = 3.04 \pm 0.08$, 3.17 ± 0.16 and 3.23 ± 0.14 nm/s, respectively).

The trend observed for the different anions tested here can be explained by considering the unfavorable entropic effect upon calcite dissolution. Ion mobility of halides in water and therefore the residence time of water in their hydration shells, increases in the order $F^- < I^- < Cl^-$, as shown by molecular dynamics simulations (Lee and Rasaiah, 1996). Hence, water is less mobile around F^- and, thus, more mobile around Ca^{2+}. Accordingly, the unfavorable entropic effect on calcite dissolution is progressively reduced in the order $Cl^- < I^- < F^-$ due to an increasing frequency of water exchange around a calcium ion, which leads to increasing dissolution kinetics in the same order. This is in agreement with the work by Pokrovsky and Schott (2002) who showed a positive correlation between dissolution rates of divalent metal carbonates and rates of water exchange around metal ions. As in the case of barite (Kowacz and Putnis, 2008), the effect of salts on calcite dissolution rate can be considered equivalent to the effect of temperature. The solvent is more structured when F^- is present (compared to I^-, Cl^- or deionized water), so this case would be similar to calcite dissolution in water at a lower temperature. Increase in temperature results in increased hydration, a negative entropic and slower dissolution (at pH > 5.5 where the dissolution rate is pH independent). Furthermore, F^- ions increase the etch pit nucleation density due to disruption of the surface hydration water, and therefore increase calcite dissolution rates.

5. CONCLUSIONS

The presence of ions in solution in contact with calcite surfaces during dissolution results in changes in both the morphology and the nucleation density of dissolution features as well as in the kinetics of the process. These observations can be explained by changes in the solvation environment of Ca^{2+} ions, disruption of the surface hydration layer and ion incorporation. Changes in etch pit morphology were observed in the presence of F^- and Li^+ that are ascribed to stabilization of etch pit edges bonded by like-charged ions due to increased hydration and ion incorporation, respectively. As previously reported and confirmed here for the case of F^-, highly hydrated ions (i.e. kosmotropes) increased the etch pit nucleation density by up to one order of magnitude compared to pure water. This may be related to a reduction in the energy barrier for etch pit nucleation due to disruption of the surface hydration layer. The relative decrease in entropy occurring during calcite dissolution in the presence of non-paired electrolytes at low IS, compared to dissolution in pure water, is due to stabilization of water molecules in the hydration shells of calcite building units. This leads to a reduction in etch pit spreading rate compared with pure water and other electrolytes which form ion-pairs in solution. At high ionic strength, the main differences in calcite dissolution kinetics are found for different background anions as they control the solvent structure around Ca^{2+} and, hence, calcium removal from the structure, the rate limiting step for dissolution. This is confirmed by the similarity of dissolution rates

in the presence of electrolytes with a common anion. Under these conditions, the calcite dissolution is reduced in the order $Cl^- < I^- < F^-$ for salts with a common cation due to an increasing frequency of water exchange around the calcium ion. These results are expected to contribute to a better understanding of how ions mediate crystal growth and dissolution reactions, which may be of importance for a wide range of processes where reactions between minerals and aqueous solutions play a role, including chemical weathering of rocks, building stone deterioration and biomineralization.

ACKNOWLEDGMENTS

This work is carried out within the EU Initial Training Network Delta-Min (Mechanisms of Mineral Replacement Reactions) Grant PITN-GA-2008-215360 and the EU Early Stage Training Network MIR (Mineral-fluid Interface Reactivity) Contract No. MEST-CT-2005-021120. Experimental facilities are supported by the Deutsche Forschungsgemeinschaft (DFG). We are thankful to Prof. Mucci, Dr. Ardvison and the two anonymous referees for their constructive comments and editing suggestions that helped us improve the overall quality and appeal of this manuscript.

REFERENCES

Arvidson R. S., Ertan I. E., Amonette J. E. and Luttge A. (2003) Variations in calcite dissolution rates: a fundamental problem? *Geochim. Cosmochim. Acta* **67**, 1623–1624.

Arvidson R. S., Collier M., Davis K. J., Vinson M. D., Amonette J. E. and Luttge A. (2006) Magnesium inhibition of calcite dissolution kinetics. *Geochim. Cosmochim. Acta* **70**, 583–594.

Barwise A. J., Compton R. G. and Unwin P. R. (1990) The effect of carboxylic acids on the dissolution of calcite in aqueous solution. Part 2. D-, L- and *meso*-tartaric acids. *J. Chem. Soc., Faraday Trans.* **86**, 137–144.

Buhmann D. and Dreybrodt W. (1987) Calcite dissolution kinetics in the system H_2O–CO_2–$CaCO_3$ with participation of foreign ions. *Chem. Geol.* **64**, 89–102.

Collins K. D. (1997) Charge density-dependent strength of hydration and biological structure. *Biophys. J.* **72**, 65–76.

Collins K. D., Neilson G. W. and Enderby J. E. (2007) Ions in water: characterizing the forces the control chemical processes and biological structure. *Biophys. Chem.* **128**, 95–104.

De Giudici G. (2002) Surface control vs. diffusion control during calcite dissolution: dependence of step-edge velocity upon solution pH. *Am. Mineral.* **87**, 1279–1285.

Dove P. M., Han N. and De Yoreo J. J. (2005) Mechanisms of classical crystal growth theory explain quartz and silicate dissolution behavior. *Proc. Natl. Acad. Sci. USA* **102**, 15357–15362.

Dove P. M. and Czank C. (1995) Crystal chemical controls on the dissolution kinetics of the isostructural sulfates: celestite, anglesite and barite. *Geochim. Cosmochim. Acta* **59**, 1907–1915.

Duckworth O. W. and Martin S. T. (2004) Dissolution rates and pit morphologies of rhombohedral carbonate minerals. *Am. Mineral.* **89**, 554–563.

Gledhill D. K. and Morse J. W. (2006) Calcite dissolution kinetics in Na–Ca–Mg–Cl brines. *Geochim. Cosmochim. Acta* **70**, 5802–5813.

Hawlicka E. and Swiatla-Wojcik D. (2003) Aggregation of ions in methanol–water solutions of sodium halides. *J. Chem. Phys.* **119**, 2206–2213.

Hay M. B., Workman R. K. and Manne S. (2003) Mechanisms of metal ion sorption on calcite: composition mapping by lateral force microscopy. *Langmuir* **19**, 3727–3740.

Kanellopoulou D. G. and Koutsoukos P. G. (2003) The calcitic marble/water interface: kinetics of dissolution and inhibition with potential implications in stone conservation. *Langmuir* **19**, 5691–5699.

Kowacz M. and Putnis A. (2008) The effect of specific background electrolytes on water structure and solute hydration: consequences for crystal dissolution and growth. *Geochim. Cosmochim. Acta* **72**, 4476–4487.

Kowacz M., Putnis C. V. and Putnis A. (2007) The effect of cation:anion ratio in solution on the mechanism of barite growth at constant supersaturation: role of the desolvation process on the growth kinetics. *Geochim. Cosmichim. Acta* **71**, 5168–5179.

Lee S. H. and Rasaiah J. C. (1996) Molecular dynamics simulation of ion mobility. 2. Alkali metal and halide ions using the SPC/E model for water at 25 °C. *J. Chem. Phys.* **100**, 1420–1425.

Liang Y., Baer D. R., McCoy J. M., Amonette J. E. and LaFemina J. P. (1996) Dissolution kinetics at the calcite–water interface. *Geochim. Cosmochim. Acta* **60**, 4883–4887.

MacInnis I. N. and Brantley S. L. (1992) The role of dislocations and surface morphology in calcite dissolution. *Geochim. Cosmochim. Acta* **56**, 1113–1126.

Marcus Y. (1987) Thermodynamics of ion hydration and its interpretation in terms of a common model. *Pure Appl. Chem.* **59**, 1093–1101.

Marcus Y. (2009) Effect of ions on the structure of water: structure making and breaking. *Chem. Rev.* **109**, 1346–1370.

Morse J. W. and Arvidson R. S. (2002) The dissolution kinetics of major sedimentary carbonate minerals. *Earth Sci. Rev.* **58**, 51–84.

Paquette J. and Reeder R. J. (1995) Relationship between surface structure, growth mechanism, and trace element incorporation in calcite. *Geochim. Cosmochim. Acta* **59**, 735–749.

Pastero L., Costa E., Bruno M., Sgualdino G. and Aquilano D. (2004) Morphology of calcite ($CaCO_3$) crystals growing from aqueous solutions in the presence of Li^+ ions. Surface behavior of the {0 0 0 1} form. *Cryst. Growth Des.* **4**, 485–490.

Pastero L., Aquilano D., Costa E. and Rubbo M. (2005) 2D epitaxy of lithium carbonate inducing growth mechanism transitions on {0 0 0 1}-K and {0 1 $\bar{1}$ 8}-S forms of calcite crystals. *J. Cryst. Growth* **275**, e1625–e1630.

Pastero L., Massaro F. R. and Aquilano D. (2007) Experimental and theoretical morphology of single and twinned crystals of Li_2CO_3 (zabuyelite). *Cryst. Growth Des.* **7**, 2749–2755.

Perez-Garrido C., Fernández-Díaz L., Pina C. M. and Prieto M. (2007) In situ AFM observations of the interaction between calcite (1 0 1 4) surfaces and Cd-bearing aqueous solutions. *Surf. Sci.* **601**, 5499–5509.

Pokrovsky O. S. and Schott J. (2002) Surface chemistry and dissolution kinetics of divalent metal carbonates. *Environ. Sci. Technol.* **36**, 426–432.

Pokrovsky O. S., Golubev S. and Schott J. (2005) Dissolution kinetics of calcite, dolomite and magnesite at 25 °C and 0 to 50 atm pCO_2. *Chem. Geol.* **217**, 239–255.

Rajam S. and Mann S. (1990) Selective stabilization of the (0 0 1) face of calcite in the presence of lithium. *J. Chem. Soc. Chem. Commun.*, 1789–1791.

Ruiz-Agudo E., Putnis C. V., Jiménez-López C. and Rodríguez-Navarro C. (2009) An AFM study of calcite dissolution in concentrated saline solutions: the role of magnesium ions. *Geochim. Cosmochim. Acta* **73**, 3201–3217.

Samoilov O. Ya. (1965) The hydration of ions in aqueous solutions. In *Structure of Aqueous Electrolyte Solutions and the Hydration of Ions*. Consultants Bureau, New York, pp. 74–106.

Samoilov O. Y. (1967) Theory of salting out from aqueous solutions. 1. General problems. *J. Struct. Chem.* **7**, 12–19.

Samoilov O. Y. (1971) Theory of salting out from aqueous solutions. 3. Dependence of salting out on characteristics of ions of salting out agent. *J. Struct. Chem.* **11**, 929–931.

Shiraki R., Rock P. A. and Casey W. H. (2000) Dissolution kinetics of calcite in 0.1 M NaCl solution at room temperature: an atomic force microscopic (AFM) study. *Aq. Geochem.* **6**, 87–108.

Stack A. G. (2009) Molecular dynamics simulations of solvation and Kink Site formation at the 0 0 1 barite–water interface. *J. Phys. Chem. C* **113**, 2104–2110.

Teng H. H. (2004) Control by saturation state on etch pit formation during calcite dissolution. *Geochim. Cosmochim. Acta* **68**, 253–262.

Teng H. H. and Dove P. M. (1997) Surface site-specific interactions of aspartate with calcite during dissolution: implications for biomineralization. *Am. Mineral.* **82**, 878–887.

Titiloye J. O., Parker S. C. and Mann S. (1993) Atomistic simulation of calcite surfaces and the influence of growth additives on their morphology. *J. Cryst. Growth* **131**, 533–545.

Vavouraki A., Putnis C. V., Putnis A. and Koutsoukos P. G. (2009) In situ AFM crystal growth and dissolution study of calcite in the presence of aqueous fluoride. *Geophys. Res. Abstr.* **11** (EGU 2009-0).

Vinson M. D. and Luttge A. (2005) Multiple length-scale kinetics: an integrated study of calcite dissolution rates and strontium inhibition. *Am. J. Sci.* **305**, 119–146.

Vinson M. D., Arvidson R. S. and Luttge A. (2007) Kinetic inhibition of calcite (1 0 4) dissolution by aqueous manganese(II). *J. Cryst. Growth* **307**, 116–125.

Weaver M. L., Qiu S. R., Hoyer J. R., Casey W. H., Nancollas G. H. and De Yoreo J. J. (2007) Inhibition of calcium oxalate monohydrate growth by citrate and the effect of the background electrolyte. *J. Cryst. Growth* **306**, 135–145.

Associate editor: Alfonso Mucci